Mater. Res. Soc. Symp. Proc. Vol. 839 © 2005 Materials Research Society **P7.1.1**

Electron Microscopy of the Operation of Nanoscale Devices

John Cumings[1], David Goldhaber-Gordon[1], A. Zettl[2,3], M.R. McCartney[4], and J. C. H. Spence[5]

[1]Department of Physics, Stanford University, Stanford, California; [2]Department of Physics, University of California, Berkeley, California; [3]Materials Sciences Division, Lawrence Berkeley National Lab, Berkeley, California; [4]Center for Solid State Science, Arizona State University, Tempe, Arizona; [5]Department of Physics and Astronomy, Arizona State University, Tempe, Arizona.

ABSTRACT

A transmission electron microscope (TEM) is much more than just a tool for imaging the static state of materials. To demonstrate this, we present work on studying the mechanical and electrical properties of carbon nanotube devices. Multiwall carbon nanotubes are concentrically stacked tubular sheets of graphite, where the spacing between each cylinder is simply the natural spacing of graphite. Using a custom-built in-situ nanomanipulation probe, we have shown that it is possible to slide the nanotube layers in a telescopic extension mode that exhibits low friction, demonstrating the potential of nanotubes as the ultimate synthetic nanobearing. During this telescopic extension, the electrical resistance of the nanotube devices increases, opening the possibility that these devices can also be used as nanoscale rheostats. We also briefly describe work on using electron holography inside a TEM to study the electric field distribution in nanotube field-emission devices and on using a nanotube itself as a biprism for electron holography. These measurements together demonstrate the wealth of information that can be obtained and frontiers that can be opened by putting operational nanodevices inside an electron microscope.

INTRODUCTION

Nanomanipulation is a powerful tool. Atomic manipulation experiments using an STM (scanning tunneling microscope) have already demonstrated that nanomanipulation can facilitate the creation of atomic-scale structures that would be difficult to form or study by any other means [1-5]. The main problem with STM is that it requires a flat, conducting surface to work on. Furthermore, the process of acquiring an image of the surface requires scanning the STM tip back and forth many times, and can it can take several minutes just to acquire a single image. Atomic force microscopy (AFM) [6] and high-speed STM [7] lift some of these limitations, but the full benefits of nanomanipulation have yet to be realized. An alternative approach is to combine the manipulation capabilities of an STM, AFM, or related scanned probe with the imaging capabilities of high-resolution TEM. This allows continuous, real-time imaging during nanomanipulation on both conducting and insulating materials.

A nanomanipulation probe, in its simplest form, could simply be thought of as an STM tip. Instead of the location of the tip being controlled by a computer which maps out the surface, control of the position and voltage of the tip is given directly to the operator. It is possible, in principle, to modify surfaces, manipulate atoms, probe the mechanical and electronic properties of nanostructures, and build nanoscale mechanical and electronic systems. A number of such nanomanipulation stages have been developed for TEM applications [8-12]. The stages allow

measurements to be carried out on delicate nanosystem geometries which are inherently not amenable to scanned probe techniques, all with real-time TEM imaging. This presents exciting opportunities for the study of physical properties of nanoscale systems, including nanotubes.

In order to perform measurements inside the TEM on individual nanotubes, it is useful to have specimens from which nanotubes protrude in great numbers. In the case of carbon nanotubes, an easy source of such material is the soft inner boule material from a multiwall carbon nanotube arc synthesis [13]. This material contains many small fibers, and when one of these fibers is broken, the broken end has many pristine multiwall nanotubes protruding from it. It is also possible to process nanotubes into tangled mats, sometimes referred to as "bucky paper" [14], and a torn edge of this bucky paper can also be used for manipulation experiments.

Either the boule fibers or the bucky paper can be broken into pieces approximately 50 μm by 500 μm. These pieces can be easily handled with tweezers and attached to the manipulation setup. In a typical setup, the nanotubes are glued in place with conductive adhesive. Sometimes a clean metal counter-electrode is used, and in this case a 50 μm-diameter gold wire serves nicely.

PEELING AND SHARPENING MULTIWALL CARBON NANOTUBES

A simple and reliable method has been developed that allows highly controlled engineering or shaping of multiwall carbon nanotubes (MWNTs) [15]. With this method average MWNTs are easily converted into ideal-geometry tapered tips for scanned probe, field emission, or biological insertion applications. The shaping process involves electrically-driven vaporization of successive layers (i.e. tube walls) of the MWNT. Outer nanotube layers are successively removed near the end of the nanotube, leaving the core nanotube walls intact and protruding from the bulk of the MWNT. This peeling and sharpening process can be repeatedly applied to the same MWNT until the very innermost small-diameter tube or tubes protrude, often with a tip radius of curvature comparable to that of a single, single-walled nanotube. The method has been demonstrated in a transmission electron microscope (TEM) configured with a custom-built mechanical/piezo manipulation stage with electrical feedthroughs to the sample.

Figure 1 shows high resolution TEM images of a conventional arc-grown MWNT at different evolutionary stages in the peeling and sharpening process. The left end of the nanotube (not seen in the image) is attached to a stationary zero-potential gold electrode. To the right (also not shown) is a larger nanotube which serves as the shaping electrode; it is attached to the manipulator whose potential can be externally controlled. Figure 1**a** shows the MWNT in its pristine, as-grown state. For Fig. 1**b**, the shaping electrode has been momentarily brought into contact with the MWNT and a carbon onion has been inadvertently transferred from the shaping electrode to the MWNT, but the applied voltage (2.4 V) and current (170 μA) are below the shaping threshold and no peeling or sharpening has taken place. For Fig. 1**c**, the shaping electrode has been brought into contact with the tip of the MWNT at 2.9 V and 200 μA; numerous layers of the MWNT have been peeled away near its end and the MWNT now has a stepped diameter and is significantly sharpened. The carbon onion has been displaced to a benign position further down the tube. We note that the newly exposed tip of the MWNT appears undamaged. For Fig. 1**d**, the peeling and sharpening process has been repeated, resulting in a MWNT with highly desirable characteristics for many nanotube applications. The dominant protruding segment now consists of a three-walled electrically conducting nanotube with a radius of just 2.5 nm. We note that although we have used an in-situ TEM configuration to document the sharpening and peeling process, this is not a requirement. The process can be performed

blind and monitored from the electrical characteristics of the nanotube alone. In addition, the shaping electrode is easily replaced by a conventional conducting substrate.

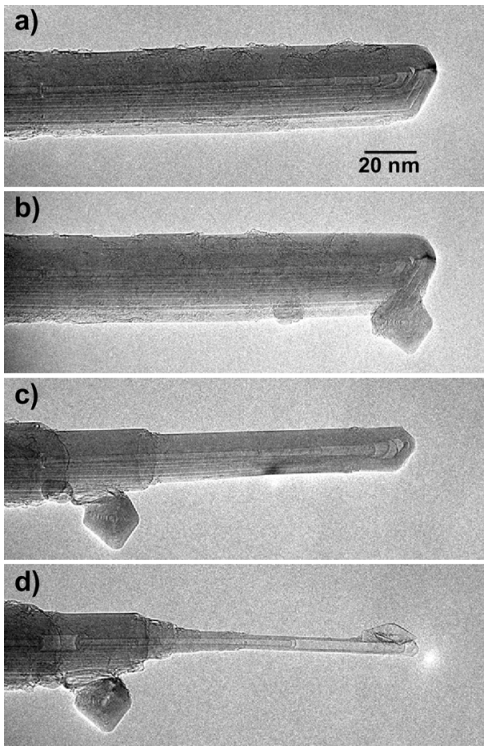

Fig. 1. Transmission electron microscope images of a multiwalled carbon nanotube being shaped: (**a**) the nanotube in its pristine form. It contains approximately 37 walls and has outer radius 12.6 nm; (**b**) a carbon onion has been inadvertently transferred to the nanotube end from the shaping electrode, but no attempt has been made to shape the nanotube; (**c**) & (**d**) the results of subsequent peeling and sharpening processes; the onion has simultaneously been displaced to a benign position down the tube axis. The shaped or "engineered" nanotube in (**d**) is thick and mechanically rigid along most of its length (not seen in the image) but tapers stepwise to a fine sharp (and electrically conducting) tip, ideal for scanned probe microscopy or electron field emission applications. The final long nanotube segment contains three walls and has outer radius 2.1 nm.

TELESCOPING NANOTUBES: LINEAR BEARINGS AND VARIABLE RESISTORS

A major difficulty in initiating controlled telescoping in MWNTs is the commonly capped ends which seal in all inner core nanotube cylinders. Even if the MWNT ends are opened by methods such as acid etching, it is difficult to selectively contact just the core tubes. One can exploit the peeling and sharpening technique described above to attach a moveable nanomanipulator [16] to only the core nanotubes within a MWNT. In-situ manipulation of the nanotube core allows controlled reversible telescoping to be achieved, and associated forces to be quantified. Robust ultra-low friction linear nanobearings and (constant-force) nanosprings are demonstrated.

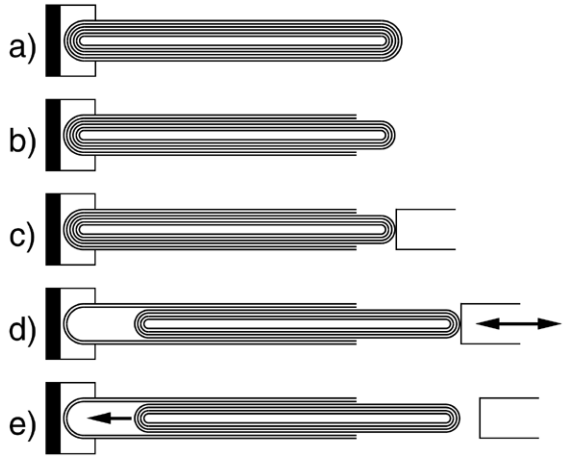

Fig. 2. A schematic representation of the experiments performed inside the TEM. Parts (**a**), (**b**), and (**c**) show the process of opening the end of a multiwall nanotube, exposing the core tubes, and attaching the nanomanipulator to the core tubes. Parts (**d**) and (**e**) depict two different classes of subsequent experiments performed. In (**d**) the nanotube is repeatedly telescoped, while observations for wear are performed. In (**e**), the core is released and pulled into the outer shell housing by the attractive van der Waals force.

Figure 2 shows schematically the configurations used inside the TEM for the different mechanical experiments. An as-grown MWNT produced by conventional arc-plasma methods is first rigidly mounted (**a**), and the free end of the MWNT is then engineered to expose the core tubes (**a**). In (**c**) the nanomanipulator is brought into contact with the core tubes and, using electrical current, is spot-welded to the core. Figure 2(**c**) is the common starting point for all of the experiments to be described here. Sub-figures (**d**) and (**e**) show two different classes of experiments. In (**d**) the manipulator is moved right and left, thus telescoping the core out from, or reinserting it into, the outer housing of nanotube shells. The extraction/reinsertion process can be repeated numerous times, all the while viewing the MWNT at high TEM resolution to test for atomic-scale nanotube surface wear and fatigue. In (**e**) the manipulator first telescopes out the inner core, then fully disengages, allowing the core to be drawn back into the outer shells by the intertube van der Waals energy-lowering force. A real-time video recording of the core bundle dynamics gives information pertaining to van der Waals and frictional forces.

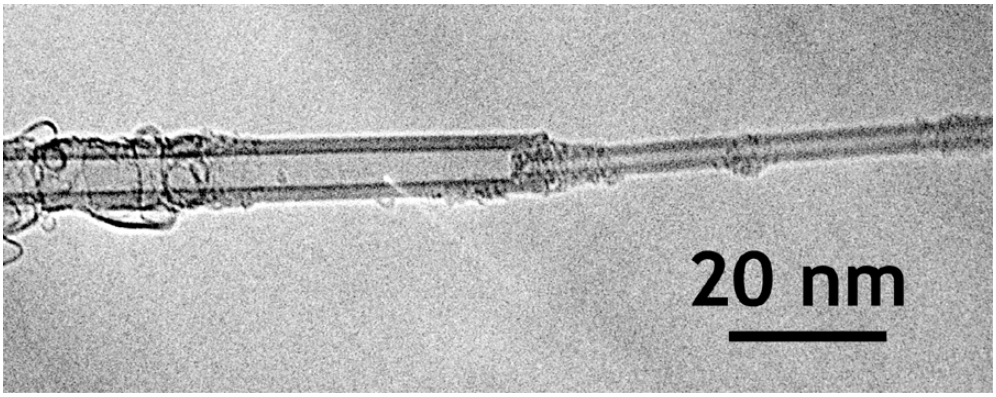

Fig. 3. A TEM image of a telescoped nanotube. This particular nanotube originally had 9 shells, but on telescoping a 4 shell core has been nearly completely extracted.

Figure 3 shows a TEM image of a MWNT in a fully telescoped position. Using higher resolution imaging than that used for Fig. 3, we determined that this MWNT originally had 9 walls, with an outer diameter of 8 nm and an inner diameter of 1.3 nm. After extension, a 4 nm diameter core segment (consisting of 4 concentric walls) has been almost completely extracted from the outer shell structure. The telescoping process was found to be fully reversible, in that the core could be completely pushed back into the outer shells, restoring the MWNT to its original retracted condition. The process of extending and retracting the core was repeated many times for several different MWNTs, and in all cases no apparent damage to the sliding surfaces, i.e. the outer tube of the core or the inner tube of the shell structure, was observed, even under the highest TEM resolution conditions (~2.5 Å). The apparent lack of induced defects or other structural changes in the nanotube contact surfaces at the atomic level suggests strongly that these near atomically-perfect nanotube structures may be wear-free and will not fatigue even after a very large number of cycles.

TELESCOPING FORCES: A LINEAR BEARING

In the engineering of macroscopic bearings, the moving parts are typically cycled 10^3 to 10^9 times before definitive conclusions about wear can be drawn. This is because the damage from a single cycle is microscopic and cannot be readily observed by eye or even conventional microscopy. Here, atomic-scale imaging of the structure is possible and shows that after all cycles, from the first cycle onward, the atomic structure of the nanotubes is unaffected by the motion. Hence it is possible to conclude that the nanotube sections are near-perfect sliding surfaces, apparently free from wear for all cycles. Interestingly, in all MWNT's that we have examined, all repeated sliding motion for a given MWNT was observed to take place between the same two nanotube shells (and similarly no multiple telescoping was observed where the total length of the nanotube might become more than double the length of the original MWNT, as would occur from sticking of the segments at some point in their extension). We interpret this repeatability as a self-selection process where the most perfect surfaces offer the least resistance to motion. Importantly, even after repeated motions, the same surfaces remained the most favored ones, again providing evidence for no sliding-induced wear on the active surfaces. (Of course, in a many-walled MWNT, even the catastrophic failure (i.e. fusing) of one surface pair would not render the MWNT bearing unusable, as another (nearly equally perfect) surface pair would simply become the active elements). In some cases, there is a small amount of residual amorphous carbon produced during the initial core exposure process. Interestingly, because of the extremely small interwall clearance in MWNTs, such contamination appears to have no effect on the bearing action as it is simply brushed away upon reinsertion of the core section into the nanotube housing. Hence, MWNT-based linear bearings are self-cleaning and immune from typical contaminant-induced wear.

Several internal forces are associated with telescoping MWNTs. To first order these consist of the van der Waals-derived force and possible static and dynamic frictional forces. The Van der Waals force is given by

$$F_{vdW}(x) = -\tfrac{\partial}{\partial x} U(x)$$

where the van der Waals energy [17] is given by U(x) = 0.16Cx joules with C the circumference of the active nanotube bearing cylinders and x the length of the overlap between the core section and the outer walls, both measured in meters. The van der Waals energy lowering gained by increasing the tube-tube contact area tends to retract the extended core of a telescoped MWNT.

Interestingly, since the active intertube contact area decreases linearly with core tube extension, this restoring force is independent of contact area, or equivalently, independent of core extension. Hence, a telescoped nanotube with only one active (sliding) surface pair is expected to act as a *constant force* spring.

To determine experimentally if F_{vdW} dominates nanotube linear bearing dynamics we have used the configuration described in Fig. 2. The core tubes of a MWNT were first telescoped using the manipulator. Lateral deflections of the manipulator were used to fatigue and eventually break the spot weld, thus releasing the core segment. The resulting accelerated motion of the released core segment was recorded using a continuous video system tied to the TEM imaging electronics.

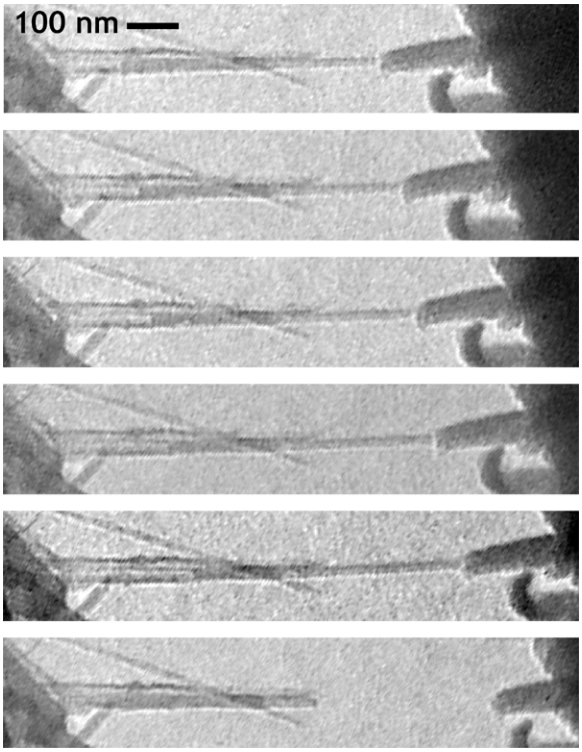

Fig. 4. Selected frames of a video recording of the in-situ telescoping of a multiwall nanotube. In the first five frames, the core nanotubes are slowly withdrawn to the right. In the sixth image, which occurred one video frame after the core was released, the core has fully retracted into the outer nanotube housing due to the attractive van der Waals force.

Figure 4 shows several selected frames from one such video recording. The upper five frames show the core segment being slowly and successively telescoped to the right (the structure in the left third of the image seen crossing the MWNT at about a 30° angle is another nanotube unrelated to the experiment and it is not in physical contact with the subject MWNT). Just after the fifth frame the manipulator has released the core segment. The sixth and final frame, which occurred one video frame after the release of the nanotube, shows the core after it rapidly and fully retracted inside the outer shells of the MWNT. The dimensions for the core segment of the MWNT of Fig. 4 yield a core segment mass 2.9×10^{-16} g. Combining this with C = 57 nm and the initial extension of 330 nm, the above equation leads to complete retraction of

the core tubes in 4.6 nsec. This is at least consistent with the experimental observation that the complete contraction occurred in less than one video frame (33 msec).

From TEM observations, we may also draw conclusions about the static and dynamic friction between concentric shells of a multiwall nanotube. While macroscopic models of friction between solids dictate that friction is proportional to normal force, independent of contact area, modern microscopic models of friction predict that friction is in fact proportional to contact area [18]. In macroscopically rough samples, the actual contact occurs at point asperities, and the microscopic contact area is proportional to the total normal force. Nanotube shells, however, are atomically smooth, so any interlocking between the shells (due, for example, to the atomic corrugations) is best estimated by using the entire surface area of contact. The F_{vdW} retraction force for the nanotube in Fig. 4 is calculated to be a mere 9 nN. This indicates that the static friction force is small, with $f_s < 2.3 \times 10^{-14}$ Newtons-per-atom (6.6×10^{-15} Newtons-per-Å). Furthermore, from the fact that the tube fully retracts, we conclude that the dynamic friction $f_k < 1.5 \times 10^{-14}$ Newtons-per-atom (4.3×10^{-15} Newtons-per-Å). Friction is an important concern in small-scale systems, such as microelectromechanical systems, or MEMS [19], and recent atomic-scale frictional force measurements [20,21] using conventional materials yield values approximately three orders of magnitude greater than the upper limit frictional forces found here for MWNT surfaces.

It is also possible to directly demonstrate through the images in Fig. 4 that the retraction force is, in fact, constant throughout the telescoping of the nanotube. The nanotube which was used as the anchor to spot weld to the tip of the core nanotube section was actually poorly anchored to the manipulator tip. It could be flexed in and out of the manipulator tip with a reasonable Hooke's law spring constant. By pushing this anchor up against a long nanotube, and using the known Young's modulus for MWNT [22], we estimated the spring constant for this nanotube deflection to be ~0.1 Newton-per-meter. In Fig. 5, we show the same images offset to that the manipulator tip (as noted by the kinked nanotube in the bottom right corner of each image) is at the same horizontal position in each frame. In these images it is possible to notice that the tip is at the same extension in each frame, implying that the retraction force is constant throughout the extension. We can also estimate the force from the spring constant to be ~5 nN, and we estimate that it is constant throughout the telescoping to within ±0.3 nano-Newton. Of course, the absolute accuracy of this order-of magnitude estimate is questionable, and is based on assumptions of linearity of the manipulator tip force response. The calculation is also subject to errors in the Young's modulus of the nanotube used to calibrate it, but it is a good order-of-magnitude estimate of the retraction force. It also demonstrates the constancy of the retraction force, and the value agrees well with the calculations in the previous paragraph, which yield 9 nano-Newtons.

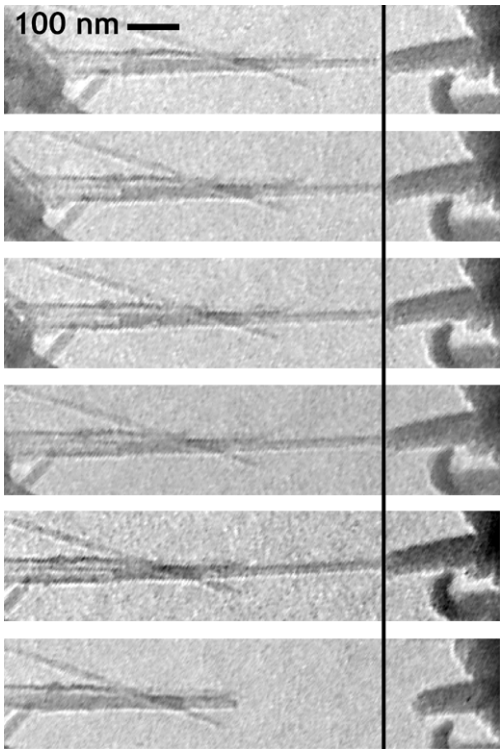

Fig. 5. The same images as Fig. 4. Here, the images have been offset to demonstrate that the anchoring nanotube, immediately to the right of the vertical line in the upper 5 images, feels a constant retraction force throughout the telescoping.

The above results demonstrate that MWNTs hold great promise for nanomechanical or nanoelectromechanical systems (NEMS) applications. Low-friction low-wear nanobearings and nanosprings are essential ingredients in general NEMS technologies. The expected order 1-10 nsec transit time for complete nanotube core retraction implies the possibility of exceptionally fast electromechanical switches.

TELESCOPING RESISTANCE: A VARIABLERESISTOR

The starting point was MWNTs whose core tubes had been partially exposed and mechanically contacted as described above. During the experiment, the dc electrical resistance between the two electrodes was monitored as the nanomanipulator reversibly telescoped the inner core tubes out from, or collapsed them back into, the outer nanotube housing.

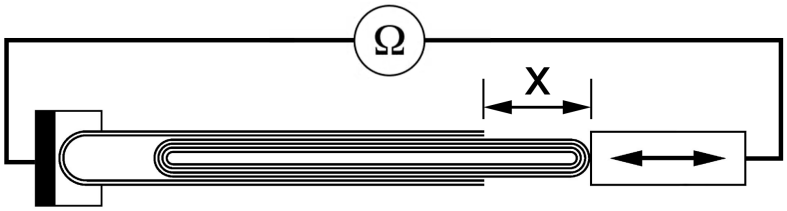

Fig. 6. Schematic diagram of telescoped MWNT resistance measurements. On the left is a nanotube anchored inside the TEM, and on the right is the manipulation tip. The nanotube is reversibly telescoped while the dc electrical resistance is measured with a low noise current amplifier.

Figure 6 shows schematically the experimental configuration. The telescoping or extraction distance x was monitored both via the nanomanipulator piezo drive voltages and analysis of direct TEM video recordings of the telescoping process. To aid in the analysis, each video frame contained critical data overlays. Throughout the telescoping process only one pair of adjacent concentric nanotube shells displayed relative motion, i.e. there was no multi-segment telescoping behavior. Typical MWNT initial (i.e. fully collapsed) lengths were from 1 to several microns. The nanotube system was always suspended in high vacuum inside the TEM (Topcon 002B, operating at 100 keV), thus eliminating potentially spurious substrate effects.

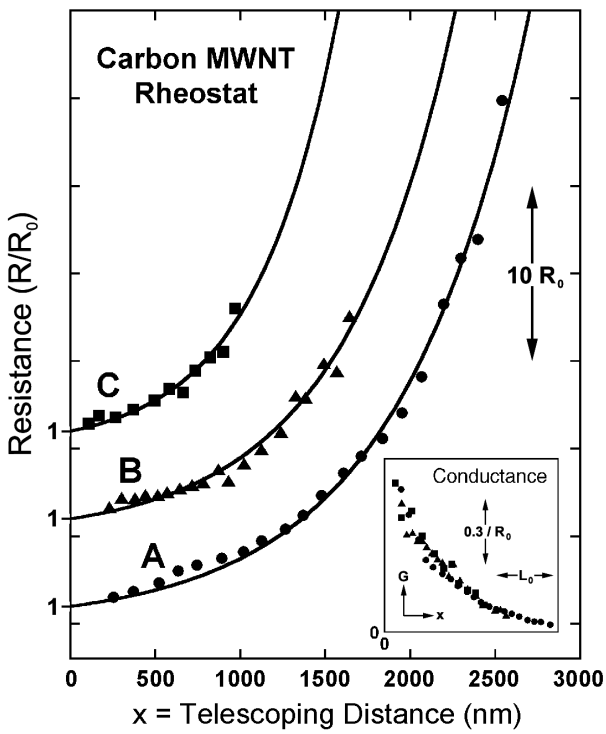

Fig. 7 Resistance R vs. telescoping distance, x, for three different nanotubes. The data are normalized to $R_0 = R(x \rightarrow 0)$. The inset shows the same data plotted as conductance (1/R) as a function of normalized telescoping distance (x/L_0). Note that the conductance data are also nonlinear and collapse onto a universal curve

Figure 7 shows, for three independent MWNTs labeled A, B, and C, the dc electrical resistance R between the ends of the telescoping nanotube system as a function of telescoping or core extraction distance x. Notice that both the resistance and the conductance are strongly nonlinear as a function of x. In [23], we attribute this nonlinear behavior to the effects of phase-coherent localization of charge carriers in the nanotube layers. This behavior is somewhat surprising because it indicates that the electrons in nanotubes maintain their quantum mechanical phase-coherence between scattering events. Such behavior requires that the electrons do not change their wavelength or loose energy between or during most scattering events. This behavior is somewhat surprising, and experiments are underway to test whether electrons lose their energy in the form of dissipated heat during transport measurements.

From a nanoscale rheostat applications viewpoint, telescoped MWNTs have attractive mechanical and electrical characteristics. They may find utility as tuning resistors, local strain gauges, or position sensors.

ELECTRON HOLOGRAPHY MEASUREMENTS OF NANOTUBES

Nanotubes have atomically-defined sharp tips, and are mechanically and thermally robust. This makes them ideal candidates for electron field emission devices, but early studies indicate strong fluctuations of the emission current for unknown reasons. In order to maximally exploit the emission characteristics of nanotubes and control undesirable fluctuations, the field emission mechanism must be understood. In particular, it would be highly desirable to quantitatively determine the actual electric field distribution surrounding a field-emitting nanotube and to correlate possible spatial and temporal fluctuations of this distribution to fluctuations in the electron emission current.

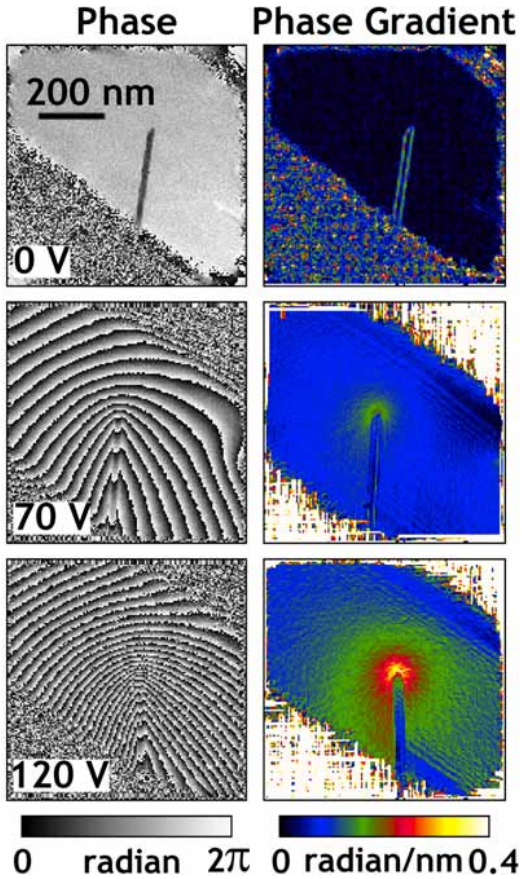

Fig. 8. Phase shift and phase gradient maps extracted from holograms of a field-emitting nanotube, as described in [24].

Electron holography is an electron interferometry technique that was developed primarily to increase the resolution of standard electron microscopy [25-27]. In addition, it can also give information about the electromagnetic fields in a specimen and we have used electron holography to study the electric fields surrounding field-emitting multiwall carbon nanotubes. Our results are reported in [24]. Briefly, we find that the nanotubes exhibit a strong field enhancement at their tips, and the electric field distribution is steady, even during times when the

emission current exhibits large fluctuations. From this we can rule out field emission from sidewall defects, nanotube-nanotube switching, and unraveling of nanotubes. Our results are consist with a fluctuating current due to the effects of gas-molecules adsorbing and desorbing from the tips of the nanotubes.

During these studies, we noticed that, under the correct conditions, the tips of the nanotubes can be observed to light-up during TEM imaging. We attribute this effect to the diffraction of the imaging electron beam by the electric field that surround the tips of the field emitting nanotubes. The effect is described in detail in [28]. In this study, we show that the effect is the same as that of a standard electrostatic biprism, and that a nanotube can be used as a biprism to perform electron holography.

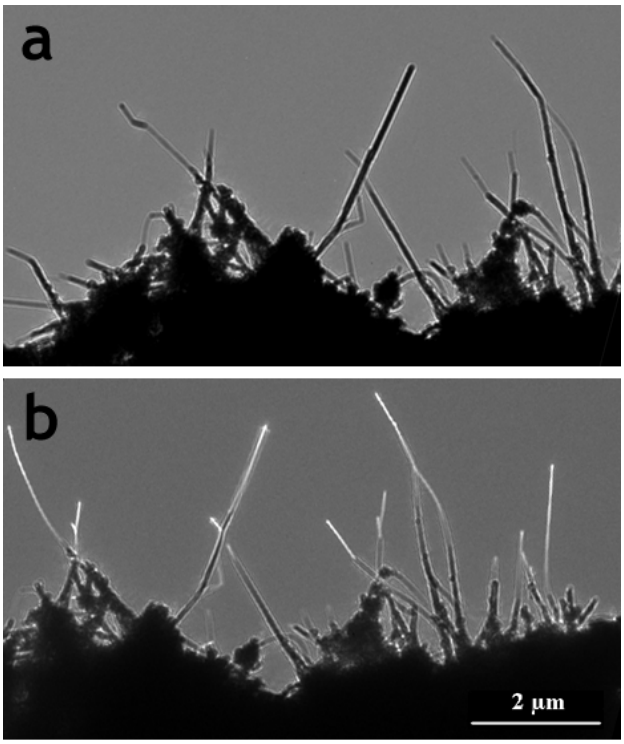

Fig. 9. Field emission from nanotubes as observed in the TEM. The images are underfocused (primarily for improved contrast). In a, the nanotubes are at ground potential. In b, the nanotubes are negatively biased relative to a counter-electrode in the field-emitting regime. Under these conditions a nanotube tip can be used as a nanoscale electrostatic biprism [28].

FUTURE DIRECTIONS

With the power of electron microscopy in imaging nanoscale devices at high speeds, the future for studying these systems is bright. We are presently developing techniques to fabricate nanoscale electronic devices on the surface of commercially available silicon nitride membranes (SPI, inc.). This will allow the investigation of a large variety of tailor-assembled nanoscale systems to be studied during operation. We are also expanding the analytical capabilities available inside a TEM to include thermal imaging. This will allow the investigation of the local generation and dissipation of heat during device operation.

ACKNOWLEDGEMENTS

We are indebted to M. L. Cohen, P. G. Collins, U. Dahmen, T. Freeman, M. S. Fuhrer, W. Q. Han, S. G. Louie, D. K. Owen and E. A. Stach for valuable contributions to the work described here.

REFERENCES

[1] G. Binnig and H. Rohrer, Helv. Physica Acta **55** 726-35 (1982)
[2] G. Binnig, H. Rohrer, C. Gerber, and E. Weibel, Phys. Rev. Lett. **50**, 120 (1983)
[3] D. M. Eigler, and E. K. Schweizer, Nature **344**, 524 (1990)
[4] M. F. Crommie, C. P. Lutz, and D. M. Eigler, D. M., Science **262**, (1993)
[5] M. T. Cuberes, R. R. Schlittler, and J. K. Gimzewski, J. K., Appl. Phys. Lett. **69**, 3016 (1996)
[6] G. Binnig, C. F. Quate, and C. Gerber, Phys. Rev. Lett. **56**, 930 (1986)
[7] R. Curtis, T. Mitsui, and E. Ganz, Rev. Sci. Instr. **68**, 2790 (1997)
[8] W. K. Lo and J. C. H. Spence, Ultramicroscopy **48,** 433 (1993)
[9] Z. L. Wang, P. Poncharal, and W. A. de Heer, J. Phys. Chem. Solids **61**, 1025 (2000)
[10] Z. L. Wang, P. Poncharal, and W. A. de Heer, W. A. Microsc. Microanal. **6**, 224 (2000)
[11] A. M. Minor, J. W. Morris, and E. A. Stach, Appl. Phys. Lett. **79**, 1625-1627 (2001)
[12] E. A. Stach, T. Freeman, A. M. Minor, D. K. Owen, J. Cumings, M. A. Wall, T. Chraska, R. Hull, J. W. Morris, A. Zettl, and U. Dahmen, Microsc. Microanal. **7,** 507 (2001)
[13] T. W. Ebbesen and P. M. Ajayan, Nature **358**, 220 (1992)
[14] A. G. Rinzler, J. Liu, H. Dai, P. Nikolaev, C. B. Huffman, F. J. Rodriguez-Macias, P. J. Boul, A. H. Lu, D. Heymann, D. T. Colbert, R. S. Lee, J. E. Fischer, A. Rao, P. C. Eklund, and R. E. Smalley, Appl. Phys. A**67**, 29 (1998)
[15] J. Cumings, P. G. Collins, and A. Zettl, Nature **406**, 586 (2000)
[16] P. Poncharal, Z. L. Wang, D. Ugarte, and W. A. De Heer, Science **283**, 1513 (1999)
[17] L. X. Benedict, N. G. Chopra, M. L. Cohen, A. Zettl, S. G. Louie, and V. H. Crespi, Chem. Phys. Lett. **286**, 490 (1998)
[18] B. N. J. Persson, Surf. Sci. Rep. **33**, 83 (1999)
[19] W. Trimmer, *Micromechanics and MEMS : classic and seminal papers to 1990* (IEEE Press, New York, 1997)
[20] R. W. Carpick, D. F. Ogletree, and M. Salmeron, Appl. Phys. Lett. **70**, 1548 (1997)
[21] M. Enachescu, R. J. A. Van Den Oetelaar, R. W. Carpick, D. F. Ogletree, C. F. J. Flipse, and M. Salmeron, Phys. Rev. Lett. **81**, 1877 (1998)
[22] M. M. J. Treacy, T. W. Ebbesen, and J. M. Gibson, Nature **381**, 678 (1996)
[23] J. Cumings and A. Zettl, Phys. Rev. Lett. **93**, 086801 (2004)
[24] J. Cumings, A. Zettl, M. R. McCartney, and J. C. H. Spence, Phys. Rev. Lett. **88**, 056804 (2002)
[25] D. Gabor, Nature **161**, 777 (1948)
[26] L. Marton, Phys. Rev. **85**, 1057 (1952)
[27] A. Orchowski, W.D. Rau, and H. Lichte, Phys. Rev. Lett. **74**, 399 (1995).
[28] J. Cumings, A. Zettl, and M. R. McCartney, Microsc. Microanal. **10**, 420 (2004)